Materials Research. 2017; 20(6): 1748-1755
DOI: http://dx.doi.org/10.1590/1980-5373-MR-2017-0377

Synthesis, Characterization and Photocatalytic Performance of SnS Nanofibers and SnSe Nanofibers Derived from the Electrospinning-made SnO_2 Nanofibers

Li Cheng[a], Dan Li[a], Xiangting Dong[a]*, Qianli Ma[a], Wensheng Yu[a], Xinlu Wang[a], Hui Yu[a], Jinxian Wang[a], Guixia Liu[a]

[a]Key Laboratory of Applied Chemistry and Nanotechnology at Universities of Jilin Province, Changchun University of Science and Technology, 130022, Changchun, China

Received: April 14, 2017; Revised: August 11, 2017; Accepted: September 04, 2017

SnO_2 nanofibers were fabricated by calcination of the electrospun PVP/$SnCl_4$ composite nanofibers. For the first time, SnS nanofibers and SnSe nanofibers were successfully synthesized by double-crucible sulfurization and selenidation methods *via* inheriting the morphology of SnO_2 nanofibers used as precursors, respectively. X-ray diffraction (XRD) analysis shows SnS nanofibers and SnSe nanofibers are respectively pure orthorhombic phase with space group of Pbnm and Cmcm. Scanning electron microscope (SEM) observation indicates that the diameters of SnS nanofibers and SnSe nanofibers are respectively 140.54±12.80 nm and 96.52±14.17 nm under the 95 % confidence level. The photocatalytic activities of samples were studied by using rhodamine B (Rh B) as degradation agent. When SnS or SnSe nanofibers are employed as the photocatalysts, the respective degradation rates of Rh B solution under the ultraviolet light irradiation after 200 min irradiation are 92.55 % and 92.86 %. The photocatalytic mechanism and formation process of SnS and SnSe nanofibers are also provided. More importantly, this preparation technique is of universal significance to prepare other metal chalcogenides nanofibers.

Keywords: *Electrospinning, SnS, SnSe, Photocatalysis, Nanofibers*

1. Introduction

In the past few decades, metal chalcogenides have attracted considerable research interest due to their outstanding semiconducting and optical properties and potential applications in future[1]. Among these materials, SnS and SnSe are increasingly important owing to their special semiconducting properties[2]. SnS is a p-type semiconductor with layered orthorhombic crystal structure. The orthorhombic herzenbergite modification of SnS consists of double layers perpendicular to *c* axis in which Sn and S atoms are tightly bound. The direct and indirect band gap of SnS were reported to be 1.2-1.5 and 1.0-1.2 eV, respectively. The narrow band gap, non-toxic nature and the interesting structure of SnS make it a potential candidate for solar absorber in thin film solar cells and semiconductor sensors[3]. Tin selenide (SnSe), as a IV-VI compound semiconductor with a band gap of about 0.9 eV, can be widely used in infrared optoelectronic devices, holographic recording systems and memory switching devices[4]. Over the past several years, the synthesis of SnS and SnSe nanomaterials has been extensively explored, and considerable efforts have been made to control the size and shape of SnS and SnSe nanomaterials[5,6].

Presently, many methods are employed to fabricate SnS and SnSe nanomaterials. Typical synthetic methods include chemical bath deposition[7-9], thermal evaporation[10,11], electrodeposition[12,13], spray pyrolysis technique[14,15], sputtering[16], *etc*. Different morphological SnS and SnSe nanomaterials were prepared by using the above methods, including nanoparticles[17,18], nanorods[19], nanoflakes[20], nanofibers[21], films[2,22], nanoplate[23], *etc*. By far, no reports on the preparation of SnS or SnSe nanofibers are found in literatures.

Conventionally, SnS or SnSe nanomaterials are prepared *via* calcination of a mixture of metal oxides or thiosulfates[7,12], thiourea[18] and sulfur powders or selenium powders at elevated temperatures. In this way, the as-prepared nanomaterials often have irregular morphology and can not inherit the peculiar morphologies of the metal oxides precursors because sulfur powders or selenium powders will melt and destroy the morphologies of the metal oxides. Hence, it is difficult to obtain metal chalcogenides nanofibers *via* direct solid-state reaction using metal oxides nanofibers as precursors. In order to solve this problem, a double-crucible method is proposed and used to retain the morphology of SnS or SnSe nanofibers using SnO_2 nanofibers as precursors. Double-crucible technique has been proved to be an efficient, convenient and simple way to fabricate nanofibers, nanobelts and hollow nanofibers[24]. Meanwhile, electrospinning is a promising, straightforward and convenient way to prepare one-dimensional (1D) nanomaterials[25-27] with diameters ranging from tens of nanometers up to micrometers owing to its easy control and low cost, including nanowires[28], nanobelts[29-31], core-shell structured nanofibers[32-34], nanofibers[35,36], nanosheets[37-39]

*e-mail: dongxiangting888@163.com

core-shell structured nanotubes[40,41], *etc.* Nevertheless, the fabrication of SnS or SnSe nanofibers *via* electrospinning combined with a double-crucible technique is not reported. Hence, fabrication of SnS or SnSe nanofibers remains a challenging and meaningful subject of study.

In this work, PVP/$SnCl_4$ composite nanofibers were fabricated by electrospinning, and SnO_2 nanofibers were prepared through calcining the as-obtained composite nanofibers at 450 ºC. For the first time, SnS or SnSe nanofibers were synthesized by a double-crucible technique we newly proposed *via* inheriting the morphology of SnO_2 nanofibers. The samples were systematically characterized. The morphology, structure and photocatalytic properties of the resulting samples were investigated in detail, and the formation mechanisms of SnS and SnSe nanofibers were also presented.

2. Experimental Sections

2.1 Chemicals

Polyvinyl pyrrolidone (K90, Mr=90000, AR), *N,N*-dimethylformamide (DMF, AR), sulfur powders and selenium powders were purchased from Tianjin Bodi Chemical Co., Ltd. $SnCl_4 \cdot 5H_2O$ was bought from China Pharmaceutical Group Shanghai Chemical Reagent Company. Distilled water was homemade.

2.2 Preparation of PVP/$SnCl_4$ composite nanofibers via electrospinning

1.00 g of $SnCl_4 \cdot 5H_2O$ was dissolved in 7.60 g of DMF, and then 1.40 g of PVP was added into the above solution under magnetic stirring for 8 h to form homogeneous transparent spinning solution. In the spinning solution, the mass ratios of PVP, $SnCl_4$ and DMF were equal to 14:10:76. Subsequently, the spinning solution was electrospun at room temperature using ordinary electrospinning setup under a positive high voltage of 13 kV, the distance between the capillary tip and the collector was fixed to 15 cm, and relative humidity was 20 %-30 %. With the evaporation of DMF, a dense web of PVP/$SnCl_4$ composite nanofibers was formed on the collector.

2.3 Synthesis of SnO_2 nanofibers

The above PVP/$SnCl_4$ composite nanofibers were calcined at 450 °C for 3 h with a heating rate of 1 °C·min^{-1}. Then the calcination temperature was decreased to 200 °C at a rate of 1 °C·min^{-1}. Finally, samples were naturally cooled down to room temperature and SnO_2 nanofibers were obtained.

2.4 Fabrication of SnS nanofibers by a double-crucible sulfurization method

2.00 g of sulfur powders were loaded into a small crucible, and then 3.00 g of carbon rods and 0.20 g of SnO_2 nanofibers were subsequently put into it. The small crucible was placed into a big crucible. Next, 2.00 g of sulfur powders were loaded into the space between the two crucibles, and then the big crucible was covered with its lid. We call this process a double-crucible method. Finally, the crucibles were heated to 800 °C with a heating rate of 5 °C·min^{-1} and remained for 4 h, then the temperature was decreased to 200 °C at a cooling rate of 2 °C·min^{-1}, followed by natural cooling down to ambient temperature. In the sulfurization process, Ar gas is used as shielding gas. Thus, SnS nanofibers were acquired.

2.5 Preparation of SnSe nanofibers via a double-crucible selenidation method

The procedure was the same as the sulfurization process, except that 5.00 g of selenium powders was used instead of sulfur powders and the selenidation reaction was conducted at 700 °C for 3 h.

2.6 Characterization methods

X-ray diffraction (XRD) analysis was performed using a Rigaku D/max-RA X-ray diffractometer with Cu kα radiation of 0.15418 nm. The size and morphology of the products were investigated by an XL-30 field emission scanning electron microscope (SEM) made by FEI Company. The purity of the products was examined by OXFORD ISIS-300 energy dispersive X-ray spectrometer (EDS) attached to the SEM. The histograms of diameters distribution were drawn by Image-Pro-Plus 6.0 and origin 8.5 softwares. All the determinations were performed at room temperature.

2.7 Evaluation of photocatalytic performance

In a typical photocatalytic reaction, 5 mL of 0.1 g·L^{-1} Rh B solution was added into 95 mL of distilled water, then 0.05 g of the as-prepared SnS and SnSe nanofibers were dispersed into the above aqueous solution of Rh B and the solution was stirred for 2 h in the dark to reach adsorption-desorption equilibrium. Then the solution was directly exposed under the ultraviolet light (500 W ultraviolet lamp with main emission wavelength of 365 nm) at an irradiation distance 20 cm with stirring to trigger decomposition of the Rh B molecules. In a 20-minute interval, 4 mL solution was sampled and centrifuged to remove the photocatalyst samples. The concentration of Rh B solution was analyzed. The degradation rate of Rh B was estimated on the basis of the following formula:

$$D\% = [(A_0 - A_t)/A_0] \times 100\%$$

where A_0 was the absorbance of Rh B in the dark and A_t was the absorbance of Rh B at given time intervals after irradiation, D was the degradation rate of the Rh B.

3. Results and Discussion

3.1 XRD analysis

Figure 1a shows the XRD patterns of SnO_2 nanofibers. All the diffraction peaks are highly consistent with those of the pure tetragonal-phase of SnO_2 (PDF#88-0287) with space group of P42/mnm. Obvious diffraction peaks are located near 2θ=26.2° (110), 33.9° (101), 37.9° (200), 51.9° (211), 54.8° (220), 62.9° (112), 65.9° (311), 78.8° (321), 83.9° (222), *etc*. No diffraction peaks of any other phases or impurities are also detected, indicating that pure-phase SnO_2 nanofibers are successfully prepared.

Figure 1b reveals the XRD patterns of SnS nanofibers, and the diffraction peaks can be easily indexed to those of the pure orthorhombic phase of SnS (PDF#75-0925), and the space group is Pbnm. Obvious diffraction peaks are situated near 2θ=25.9° (201), 25.6° (210), 31.8° (111), 37.0° (311), 44.8° (411), 51.2° (121), 66.2° (800), 75.6° (811), 84.2° (820), *etc.* No peaks of any other phases or impurities are also detected, implying that crystalline SnS is acquired.

Figure 1c manifests shows the XRD patterns of SnSe nanofibers. Its reflection peaks can be readily indexed to those of the pure orthorhombic phase of SnSe (PDF#53-0527), and the space group is Cmcm. Obvious diffraction peaks are located near 2θ=15.5° (002), 26.5° (012), 28.5° (110), 31.0° (004), 38.0° (014), 43.2° (202), 44.2° (115), 47.6° (022), 49.6° (115), *etc*. No peaks of any other phases or impurities are detected, indicating that crystalline SnSe is obtained.

3.2 Morphology observation

The morphologies of the products are characterized by scanning electron microscope (SEM). Figure 2 manifests the representative SEM images of PVP/$SnCl_4$ composite nanofibers, SnO_2 nanofibers, SnS nanofibers and SnSe nanofibers. From Figure 2a, it can be noticed that PVP/$SnCl_4$ composite nanofibers have smooth surface and uniform diameter. After calcination at 450 °C, the diameter of SnO_2 nanofibers greatly decreases due to loss of the PVP and associated organic components, as revealed in Figure 2b. SnS nanofibers and SnSe nanofibers have relatively rough surface, as seen in Figure 2c and 2d. From these analyses, we can safely conclude that the double-crucible technique we proposed here can remain the morphology of the SnO_2 precursor nanofibers.

Histograms of diameters of these fibers are indicated in Figure 3. Under the 95 % confidence level, the diameters of fibers analyzed by Shapiro-Wilk method are normal distribution. The diameters of PVP/$SnCl_4$ composite nanofibers, SnO_2 nanofibers, SnS nanofibers and SnSe nanofibers are 255.55±23.73 nm, 63.56±6.74 nm, 140.54±12.80 nm and 96.52±14.17 nm, respectively.

Figure 4 demonstrates the EDS spectra of PVP/$SnCl_4$ composite nanofibers, SnO_2 nanofibers, SnS nanofibers and SnSe nanofibers. EDS spectra analysis shows that C, N, O, Sn, Cl are the main elements in PVP/$SnCl_4$ composite nanofibers and the presence of Sn, O corresponds to SnO_2 nanofibers, as seen in Figure 4a and 4b. Sn, S are the main elements in SnS nanofibers and the presence of Sn, Se corresponds to SnSe nanofibers, as indicated in Figure 4c and 4d, C exists in SnS and SnSe nanofibers due to carbon rods loaded into the small crucible during the sulfurization and selenidation process, Pt comes from the conductive films coated on the samples for SEM analysis, and the O is owing to absorbed oxygen.

3.3 Photocatalytic properties

The photocatalytic activity of the SnO_2 nanofibers, SnS nanofibers and SnSe nanofibers were evaluated by the degradation of Rh B solution under ultraviolet irradiation, as seen in Figure 5. Figure 5 displays the degradation curves of Rh B solution and first-order reaction kinetics curves. The degradation rate of Rh B solution reaches 85.90 % using SnO_2 nanofibers after 180 min irradiation. While SnS nanofibers or SnSe nanofibers are employed as the photocatalysts, the respective degradation rates of Rh B solution after 200 min

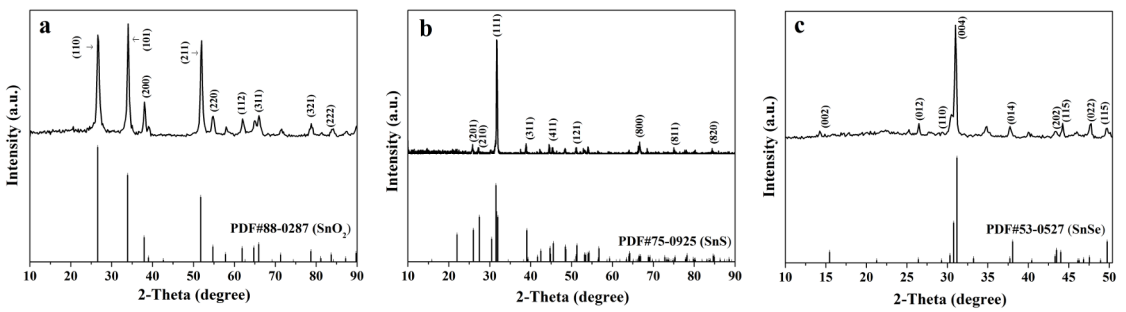

Figure 1. XRD patterns of SnO_2 nanofibers (a), SnS nanofibers (b) and SnSe nanofibers (c) with PDF standard cards of SnO_2, SnS and SnSe.

irradiation are 92.55 % and 92.86 %. Degradation of Rh B solution accords with the first-order reaction kinetics equation:

$$\ln\left(\frac{C}{C_0}\right) = -K(t - t_0)$$

where C_0 is the initial concentration of Rh B solution, C is the concentration of Rh B solution at given time intervals after irradiation, K is the rate constant, t_0 is the initial irradiation time and t is the irradiation time. The rate constant K of SnO_2 nanofibers, SnS nanofibers and SnSe nanofibers are K_1=0.00988 s^{-1}, K_2=0.01336 s^{-1} and K_3=0.01357 s^{-1}, respectively.

3.4 Possible mechanism of the ultraviolet-induced photodegradation of Rh B

Based on the above results, a possible photocatalytic mechanism is indicated in Figure 6. As shown in Figure 6, SnS nanofibers and SnSe nanofibers with narrow band gap energy (*ca.* 1.01 eV and 0.90 eV) could be easily excited by ultraviolet light to generate photoelectrons and holes. Then the photo-generated electrons (e^-) probably react with dissolved oxygen molecules to yield super oxide radical anions $O_2^{\cdot -}$, which on protonation forms the hydroperoxy $HO_2^{\cdot}$ and the hydroxyl radical OH^-. Simultaneously, the holes (h^+) could oxidize OH^- and H_2O to generate $OH^{\cdot}$. $HO_2^{\cdot}$ and $OH^{\cdot}$ which are strong oxidizing agent could make C-C, C-O and C-H in Rh B molecule rupture to form harmless CO_2 and H_2O.

4. Formation Mechanisms for SnS Nanofibers and SnSe Nanofibers

On the basis of above analytic of results, we propose the formation mechanisms for SnS nanofibers and SnSe nanofibers, as shown in Figure 7. PVP and $SnCl_4$ were mixed with DMF to form spinning solution with certain viscosity. Then, PVP/$SnCl_4$ composite nanofibers were obtained *via* electrospinning. During calcination process, PVP chain was broken and volatilized. With the increase in calcination temperature, Sn^{4+} was oxidized to form SnO_2 crystallites, many crystallites were combined into nanoparticles, then some nanoparticles were mutually connected to generate SnO_2 nanofibers. PVP acted as template during the formation of SnO_2 nanofibers. It was found from experiments that the average molecular weight and content of PVP in the spinning solution played important roles in the formation of SnO_2 nanofibers. Next, SnO_2 nanofibers were sulfurized and selenided using S and Se powders as sulfurizing and

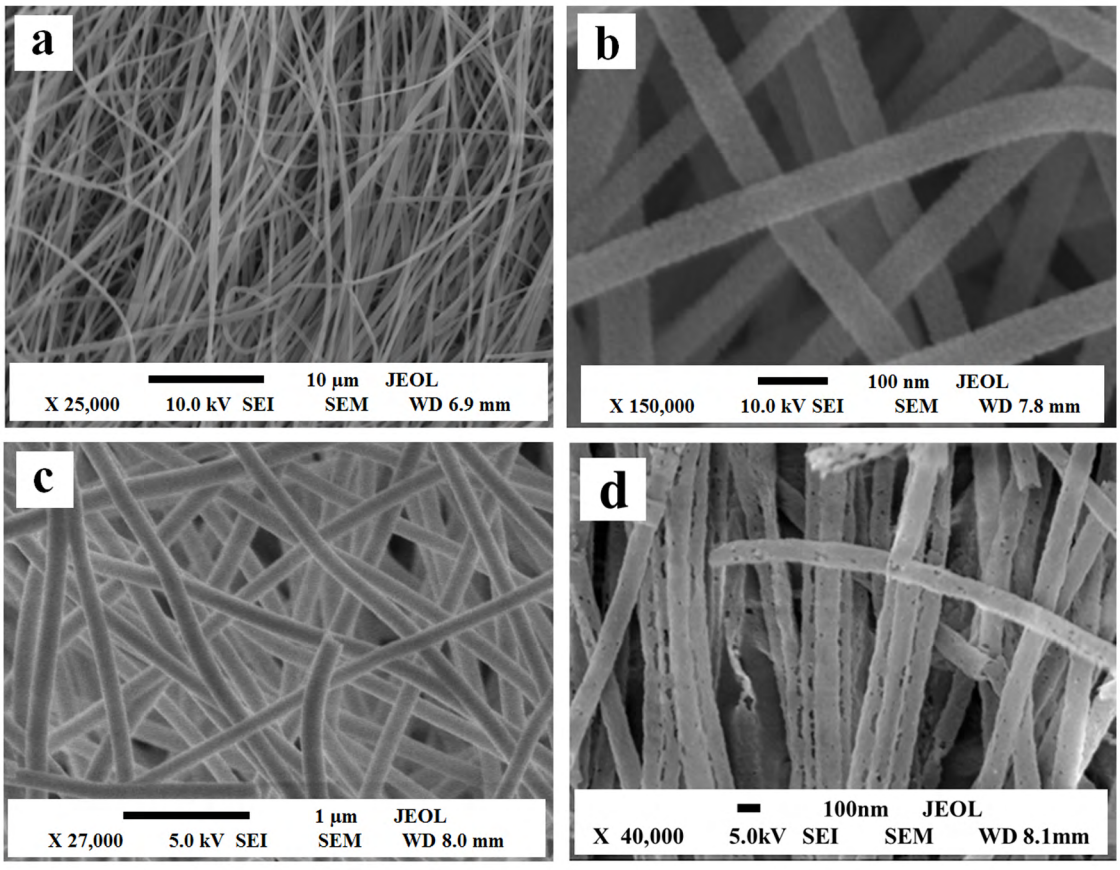

Figure 2. SEM images of PVP/$SnCl_4$ composite nanofibers (a), SnO_2 nanofibers (b), SnS nanofibers (c) and SnSe nanofibers (d).

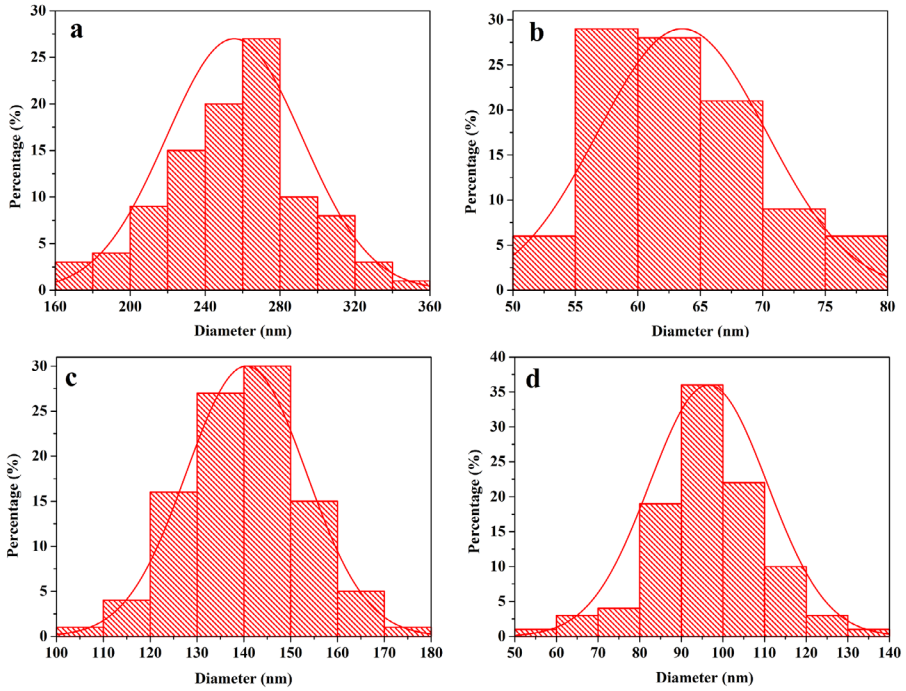

Figure 3. Histograms of diameters of PVP/$SnCl_4$ composite nanofibers (a), SnO_2 nanofibers (b), SnS nanofibers (c) and SnSe nanofibers (d).

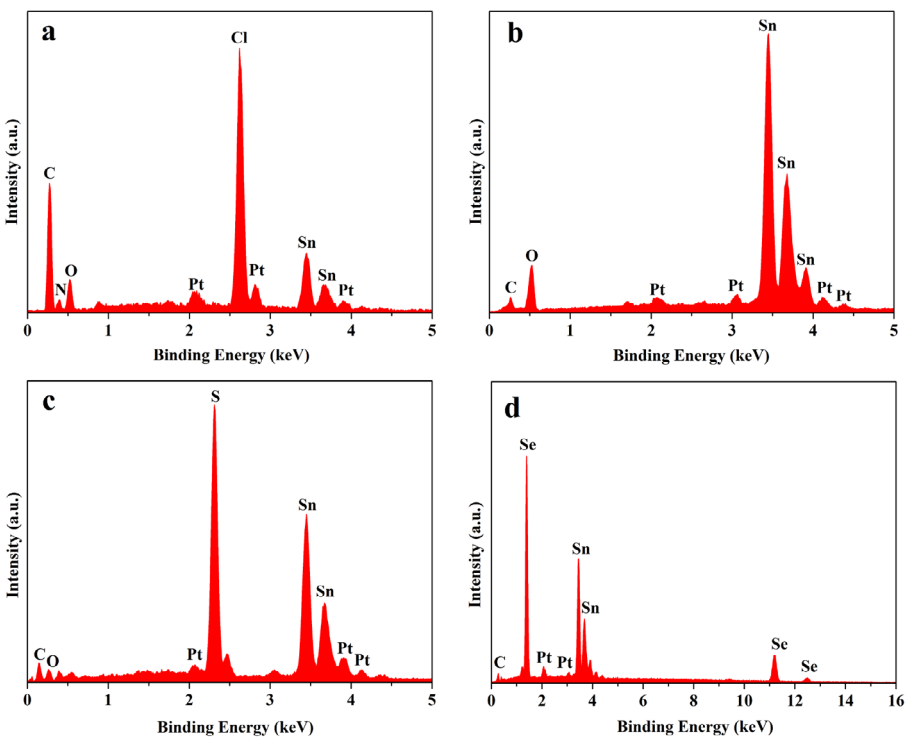

Figure 4. EDS spectra of PVP/$SnCl_4$ composite nanofibers (a), SnO_2 nanofibers (b), SnS nanofibers (c) and SnSe nanofibers (d).

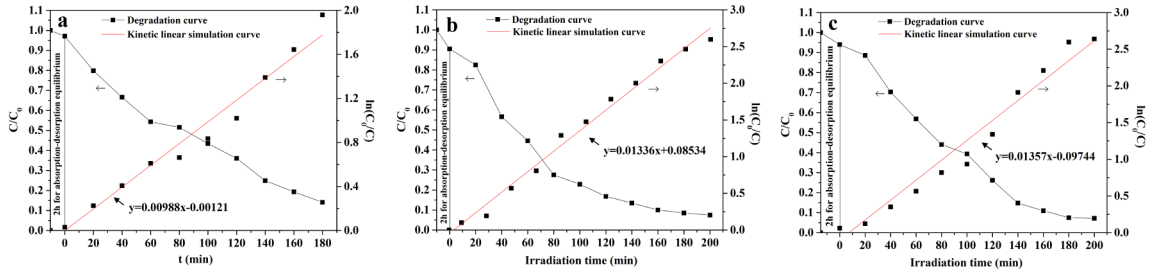

Figure 5. Variation of degradation curves of Rh B with irradiation time over SnO_2 nanofibers (a), SnS nanofibers (b) and SnSe nanofibers (c).

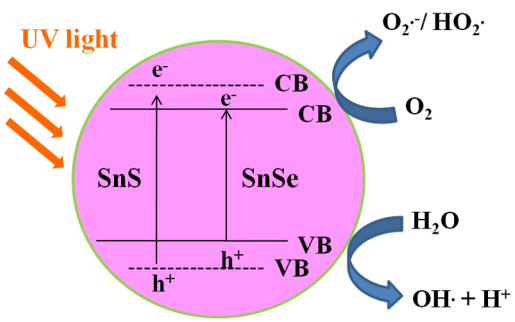

Figure 6. Possible mechanism of the ultraviolet-induced photodegradation of Rh B with SnS nanofibers and SnSe nanofibers.

seleniding agents. In the process, S or Se reacted with SnO_2 nanofibers to produce SnS nanofibers or SnSe nanofibers. During the process, S or Se powders and SnO_2 nanofibers were separated by the carbon rods, which prevented SnO_2 nanofibers from morphology damage. If SnO_2 nanofibers directly mix with S or Se powders, melted S or Se will cut the SnO_2 nanofibers into pieces, as a result, the morphology of SnO_2 nanofibers cannot be retained. Carbon rods played an important role in the reduction via combination with O_2 to produce CO, which reacted with oxygen species of SnO_2 to give CO_2 in the heating process. The double-crucible method we proposed here is actually a solid-gas reaction, which has been proved to be an important method, not only can retain the morphology of SnO_2 nanofibers, but also can fabricate SnS nanofibers and SnSe nanofibers with pure phase at relatively low temperature. Reaction schemes for formation of SnS nanofibers or SnSe nanofibers proceeded as follows:

$$PVP/SnCl_4 + O_2 \xrightarrow{450°C} CO_2 + H_2O + HCl + SnO_2 \quad (1)$$

$$2C + O_2 \longrightarrow 2CO \quad (2)$$

$$SnO_2 + S + 2CO \xrightarrow{800°C} SnS + 2CO_2 \quad (3)$$

$$SnO_2 + Se + 2CO \xrightarrow{700°C} SnSe + 2CO_2 \quad (4)$$

5. Conclusions

In summary, SnO_2 nanofibers were fabricated by calcination of PVP/$SnCl_4$ composite nanofibers prepared *via* electrospinning, and pure-phase orthorhombic SnS nanofibers or SnSe nanofibers with space group of Pbnm or

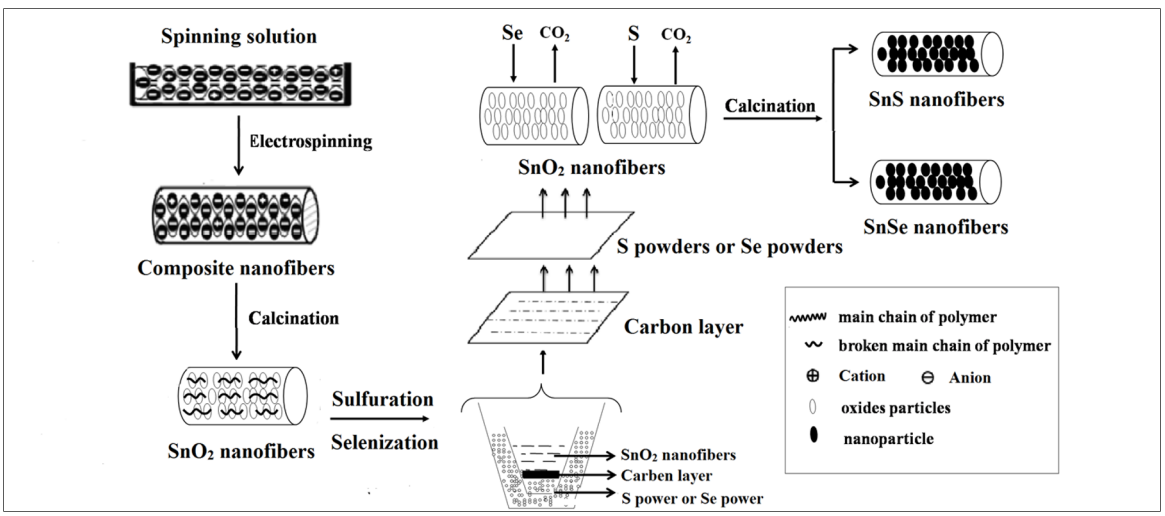

Figure 7. Formation mechanisms of SnS nanofibers and SnSe nanofibers.

Cmcm were obtained by sulfuration or selenization of the as-obtained SnO_2 nanofibers. The as-prepared SnS nanofibers and SnSe nanofibers have relatively rough surface, their diameters are respectively 140.54±12.80 nm and 96.52±14.17 nm. SnS nanofibers and SnSe nanofibers possess excellent photocatalytic performance. The double-crucible technology we proposed here is of great importance, it can be applicable to synthesize other metal chalcogenides nanostructures with various morphologies.

6. Acknowledgments

This work was financially supported by National Natural Science Foundation of China (51573023, 50972020), Natural Science Foundation of Jilin Province of China (20170101101JC), Industrial Technology Research and Development Project of Jilin Province Development and Reform Commission (2017C051), Science and Technology Research Planning Project of the Education Department of Jilin Province during the 13th Five-Year Plan Period (JJKH20170608KJ), Youth Foundation of Changchun University of Science and Technology (No. XQNJJ-2016-01).

7. References

1. Tang H, Yu JG, Zhao X. Solvothermal synthesis of novel dendrite-like SnS particles in a mixed solvent of ethylenediamine and dodecanethiol. *Journal of Alloys and Compounds*. 2008;460(1-2):513-518.

2. Park JP, Song MY, Jung WM, Lee WY, Lee JH, Kim HG, et al. Preparation of SnS Thin Films by MOCVD Method Using Single Source Precursor, Bis(3-mercapto-1-propanethiolato) Sn(II). *Bulletin of the Korean Chemical Society*. 2012;33(10):3383-3386.

3. Zhang H, Hu C, Wang X, Xi Y, Li X. Synthesis and photosensitivity of SnS nanobelts. *Journal of Alloys and Compounds*. 2012;513:1-5.

4. Sharma J, Singh G, Thakur A, Saini GSS, Goyal N, Tripathi SK. Preparation and characterization of SnSe nanocrystalline thin films. *Journal of Optoelectronics and Advanced Materials*. 2005;7(4):2085-2094.

5. Hsu KC, Wu DY, Lin PY, Fu YS, Liao JD. Molecular assessment of histopathological staging in squamous-cell carcinoma of the head and neck. *Journal of Applied Polymer Science*. 2015;33:132-137.

6. Nassary MM. The electrical conduction mechanisms and thermoelectric power of SnSe single crystals. *Turkish Journal of Physics*. 2009;33(4):201-208.

7. Gao C, Shen H. Influence of the deposition parameters on the properties of orthorhombic SnS films by chemical bath deposition. *Thin Solid Films*. 2012;520(9):3523-3527.

8. Mukherjee A, Mitra P. Characterization of tin (II) sulphide thin film synthesized by successive chemical solution deposition. *Indian Journal of Physics*. 2015;89(10):1007-1012.

9. He HY, Fei J, Lu J. Rapid Chemical Bath Depositions and Properties of SnS Films. *Materials and Manufacturing Processes*. 2014;29(9):1044-1049.

10. Kawano Y, Chantana J, Minemoto T. Impact of growth temperature on the properties of SnS film prepared by thermal evaporation and its photovoltaic performance. *Current Applied Physics*. 2015;15(8):897-901.

11. Abdelrahman AE, Yunus WMM, Arof AK. Optical properties of tin sulphide (SnS) thin film estimated from transmission spectra. *Journal of Non-Crystalline Solids*. 2012;358(12-13):1447-1451.

12. Mariappan R, Mahalingam T, Ponnuswamy V. Preparation and characterization of electrodeposited SnS thin films. *Optik - International Journal for Light and Electron Optics*. 2011;122(24):2216-2219.

13. Steichen M, Djemour R, Gütay L, Guillot J, Siebentritt S, Dale PJ. Direct synthesis of single-phase p-type SnS by electrodeposition from a dicyanamide Ionic liquid at high temperature for thin film solar cells. *Journal of Physical Chemistry C*. 2013;117(9):4383-4393.

14. Reddy NK, Reddy KTR. Preparation and characterisation of sprayed tin sulphide films grown at different precursor concentrations. *Materials Chemistry and Physics*. 2007;102(1):13-18.

15. Akbari T, Rozati SM. Preparation and growth of SnS thin film deposited by spray pyrolysis technique. *Chemistry of Solid Materials*. 2014;2(1):33-39.

16. Chao J, Xie Z, Duan X, Dong Y, Wang Z, Xu J, et al. Visible-light-driven photocatalytic and photoelectrochemical properties of porous SnS_x (x= 1,2) architectures. *CrystEngComm*. 2012;14(9):3163-3168.

17. Gou XL, Chen J, Shen PW. Synthesis, characterization and application of SnS_x (x = 1, 2) nanoparticles. *Materials Chemistry and Physics*. 2005;93(2-3):557-566.

18. Muthuvinayagam A, Viswanathan B. Hydrothermal synthesis and LPG sensing ability of SnS nanomaterial. *Indian Journal of Chemistry*. 2015;54A:155-160.

19. An C, Tang K, Jin Y, Liu Q, Chen X, Qian Y. Shape-selected synthesis of nanocrystalline SnS in different alkaline media. *Journal of Crystal Growth*. 2003;252(4):581-586.

20. Du M, Yin X, Gong H. Effects of triethanolamine on the morphology and phase of chemically deposited tin sulfide. *Materials Letters*. 2015;152:40-44.

21. Shen Z, Hu Y, Chen Y. Tin nanoparticle-loaded porous carbon nanofiber composite anodes for high current lithium-ion batteries. *Journal of Power Sources*. 2015;278:660-667.

22. Sun YF, Cheng H, Gao S, Sun ZH, Liu QH, Liu Q, et al. Freestanding Tin Disulfide Single-Layers Realizing Efficient Visible-Light Water Splitting. *Angewandte Chemie*. 2012;51(35):8727-8731.

23. Rath T, Gury L, Sánchez-Molina I, Martínez L, Haque SA. Formation of porous SnS nanoplate networks from solution and their application in hybrid solar cells. *Chemical Communications*. 2015;51(50):10198-10201.

24. Kong Q, Wang J, Dong X, Yu W, Liu G. Synthesis and luminescence properties of LaOCl:Eu^{3+} nanostructures via the combination of electrospinning with chlorination technique. *Journal of Materials Science: Materials in Electronics*. 2013;24(12):4745-4756.

25. Hou Z, Li G, Lian HZ, Lin J. One-dimensional luminescent materials derived from the electrospinning process: preparation, characteristics and application. *Journal of Materials Chemistry*. 2012;22(12):5254-5276.

26. Tian J, Ma Q, Dong X, Yang M, Yang Y, Wang J, et al. Flexible composite nanobelts: facile electrospinning construction, structure and color-tunable photoluminescence. *Journal of Materials Science: Materials in Electronics*. 2015;26(11):8413-8420.

27. Hou Z, Li C, Yang J, Lian H, Yang P, Chai R, et al. One-dimensional $CaWO_4$ and $CaWO_4$:Tb^{3+} nanowires and nanotubes: electrospinning preparation and luminescent properties. *Journal of Materials Chemistry*. 2009;19(18):2737-2746.

28. Ma Q, Wang J, Dong X, Yu W, Liu G. Flexible ribbon-shaped coaxial electrical Conductive nanocable array endowed with magnetism and photoluminescence. *RSC Advances*. 2015;5(4):2523-2530.

29. Han C, Ma Q, Dong X, Yu W, Wang J, Liu G. In situ synthesis of porous Fe_3O_4/C composite nanobelts with tunable magnetism, electrical conduction and highly efficient. adsorption characteristics. *Journal of Materials Science: Materials in Electronics*. 2015;26(4):2457-2465.

30. Liu Y, Wang JX, Dong XT, Liu GX. Fabrication of $Gd_3Ga_5O_{12}$:Eu^{3+} Porous Luminescent Nanobelts via Electrospinning. *Chemical Journal of Chinese Universities*. 2010;31(7):1291-1296.

31. Xue H, Sun X, Bi J, Wang T, Han J, Ma Q, et al. Facile electrospinning construction and characteristics of coaxial nanobelts with simultaneously tunable magnetism and color-tuned photoluminescence bifunctionality. *Journal of Materials Science: Materials in Electronics*. 2015;26(1):8774-8783.

32. Hou Z, Li C, Ma P, Cheng Z, Li X, Zhang X, et al. Up-Conversion Luminescent and Porous $NaYF_4$:Yb^{3+}, Er^{3+}@SiO_2 Nanocomposite Fibers for Anti-Cancer Drug Delivery and Cell Imaging. *Advanced Functional Materials*. 2012;22(13):2713-2722.

33. Ma Q, Wang J, Dong X, Yu W, Liu G, Xu J. Electrospinning preparation and properties of magnetic-photoluminescent bifunctional coaxial nanofibers. *Journal of Materials Chemistry*. 2012;22(29):14438-14442.

34. Liu Z, Sun DD, Guo P, Leckie JO. An efficient bicomponent TiO_2/SnO_2 nanofiber photocatalyst fabricated by electrospinning with a side-by-side dual spinneret method. *Nano Letters*. 2007;7(4):1081-1085.

35. Yang F, Ma Q, Dong X, Yu W, Wang J, Liu G. A novel scheme to obtain tunable fluorescent colors based on electrospun composite nanofibers. *Journal of Materials Science: Materials in Electronics*. 2015;26(1):336-344.

36. Zhou X, Ma Q, Dong X, Wang J, Yu W, Liu G. Dy^{3+} and Eu^{3+} complexes co-doped flexible composite nanofibers to achieve tunable fluorescent color. *Journal of Materials Science: Materials in Electronics*. 2015;26(5):3112-3118.

37. Wang K, Shao C, Li X, Zhang X, Lu N, Miao F, et al. Hierarchical heterostructures of p-type BiOCl nanosheets on electrospun n-type TiO_2 nanofibers with enhanced photocatalytic activity. *Catalysis Communications*. 2015;67:6-10.

38. Wang K, Shao C, Li X, Miao F, Lu N, Liu Y. Heterojunctions of p-BiOI Nanosheets/n-TiO_2 Nanofibers: Preparation and Enhanced Visible-Light Photocatalytic Activity. *Materials (Basel)*. 2016;9(2):90.

39. Zhang Z, Shao C, Li X, Sun Y, Zhang M, Mu J, et al. Hierarchical assembly of ultrathin hexagonal SnS_2 nanosheets onto electrospun TiO_2 nanofibers: enhanced photocatalytic activity based on photoinduced interfacial charge transfer. *Nanoscale*. 2013;5(2):606-618.

40. Zhang P, Wang L, Zhang X, Shao CL, Hu J, Shao G. SnO_2-core carbon-shell composite nanotubes with enhanced photocurrent and photocatalytic performance. *Applied Catalysis B: Environmental*. 2015;166-167:193-201.

41. Miao F, Shao C, Li X, Wang K, Lu N, Liu Y. Electrospun carbon nanofibers/carbon nanotubes/polyaniline ternary composites with enhanced electrochemical performance for flexible solid-State supercapacitors. *ACS Sustainable Chemistry & Engineering*. 2016;4(3):1689-1696.